*Progress In Electromagnetics Research C, Vol. 103, 199–209, 2020*

# Cracks Characterization of Non-Ferromagnetic Material Using EMAT Probe and PLSR Technique

**Houssem Boughedda[1, *], Tarik Hacib[1], Yann Le Bihan[2], and Hulusi Acikgoz[3]**

**Abstract**—The aim of this research is to propose a new efficient and reliable approach on the field of Non Destructive Testing (NDT), for the characterization of cracks in non-ferromagnetic material by Electromagnetic Acoustic Transducer (EMAT). EMAT is an ultrasonic technique that generates and detects ultrasonic waves in the conductive material without physical contact. The research goes through two principal phases. The first, which is a forward model, is based on Finite Element Method (FEM). The FEM is applied to simulate the EMAT response (output voltage) to the material under test in order to build a database for the inversion tool. The second is the inverse model and depends on the Partial Least Square Regression (PLSR) method, as it is a fast, simple, and accurate inversion tool, in order to estimate the depth and width of the cracks on the surface of non-ferromagnetic materials. PLSR is a dimensionality reduction method which aims to model the relationship between the matrix of independent variables (predictors) ($\boldsymbol{X}$) and the matrix of dependent variables (response) ($\boldsymbol{Y}$). The purpose of PLSR is to find the Latent Variables (LV) that have a higher ability of prediction by projecting original predictors into a new space of reduced dimensions.

## 1. INTRODUCTION

The need for metal structures inspection, during the production or maintenance, became an indispensable process. In some fields, such as the aeronautical, aerospace, and gas pipeline industries, the application of Non-Destructive Testing (NDT) techniques is considered as the borderline between life and death [1]. The Electromagnetic Acoustic Transducer (EMAT) is among the NDT techniques, which depends on the transmission and reception of ultrasonic waves inside a conductive material. EMAT structure consists of two main components, a magnet and a coil. This structure is mostly the same whether the EMAT functions as a transmitter or as a receiver [2–4]. One of the most important advantages of an EMAT system is the ability to generate different types of waves inside the material by a simple change in its structure or its frequency of excitation. Moreover, the monitoring of the materials by EMAT is not limited only to the inspection of the surface cracks as in Eddy Current (EC) sensor, but it can also effectively detect hidden defects with long-range sensibility [5, 6].

EMAT system has been extensively investigated by a number of researchers [7–10]. Most researches and studies have focused on the detection of the defect existence and the different types of waves that generate inside the material under test. However, the defect size and the amount of damage that can be caused by that defect did not receive much concern. EMAT system is able to sense the existence of the defect through the changes in the received signal [11]. Although this signal gives us a reading on the existence of the defect in the material, we cannot diagnose the defect dimension and its consequences. So, that is considered as one of the significant downsides of EMAT technique.

*Received 31 January 2020, Accepted 27 June 2020, Scheduled 9 July 2020*
* Corresponding author: Houssem Boughedda (houssem.boughedda@univ-jijel.dz).
[1] L2EI Laboratory, Jijel University, BP 98 Ouled Aissa, Jijel 18000, Algeria. [2] Group of Electrical Engineering — Paris (GeePs), CNRS, CentraleSupélec, Université Paris-Sud, Gif-sur-Yvette, France. [3]Engineering Faculty, Karatay University, Konya, Turkey.

The main contribution of the present work counts on proposing an efficient approach in order to estimate the size of defects in non-ferromagnetic materials. This work involves creating a database of the EMAT response to various cracks' sizes (the database includes a set of received echo signals and the defect dimensions corresponding to each signal), as a forward model. Then, solving the inverse problem via applying the Partial Least Square Regression (PLSR) method on the measured signal by EMAT to determine the depth and width of the crack in the material under test [12, 13]. The various stages of this study are summarized in the following steps. First, the evaluation of the Lorentz force is produced through the interaction of the static magnetic field and the eddy current in the material under test. Then, ultrasonic sound waves are generated in a transient elastic-dynamic model by the Lorentz force. Next, the output voltage signal is recorded on different forms of defects, in order to assess the EMAT sensitivity to the change in the defect size. The following step is the creation of a database for training the PLS model to respond to various output signals. Finally, PLSR technique, combined with the forward model, is applied on the measured output signal with indeterminate defect size, as a way to deduce the geometric parameters of the defect, such as the depth and width.

## 2. THE EMAT CONFIGURATION AND WORKING PRINCIPLE

The Electromagnetic Acoustic Transducer (EMAT) configurations differ depending on the nature of the waves that we want to generate during the inspection. Nevertheless, the principal structure of EMAT is composed of a permanent magnet, a coil, and a test specimen [14]. The EMAT structure, which is used in this work, is shown in Figure 1. It consists of a permanent magnet above six meander line coils and a non-ferromagnetic material represented in an aluminum plate. It is widely known that the Lorentz force has a major contribution in non-ferromagnetic materials, while in ferromagnetic materials, the magnetostrictive force contributes more [15]. Thus, the EMAT transduction mechanism in the aluminum plate is known as the Lorentz force. The latter has been produced at the surface of the aluminum plate via the interaction between the static magnetic field and eddy current. The static magnetic field derives from the EMAT permanent magnet, and the eddy current is induced at the surface of the material by the dynamic magnetic field of the coil which is excited by the alternative current $i_k(t)$. The Lorentz force generates the ultrasonic wave at the surface of the aluminum plate, called the Rayleigh wave, which leads to launching a mechanical vibration of the particles at the same frequency of the excitation source. In the receiving mode, the magnetic flux density, which comes from the EMAT receiver, interacts with the velocity of the mechanical displacement in the conductive material to generate spatial eddy currents underneath the receiver. These currents induce a voltage in the coil of the EMAT receiver [8].

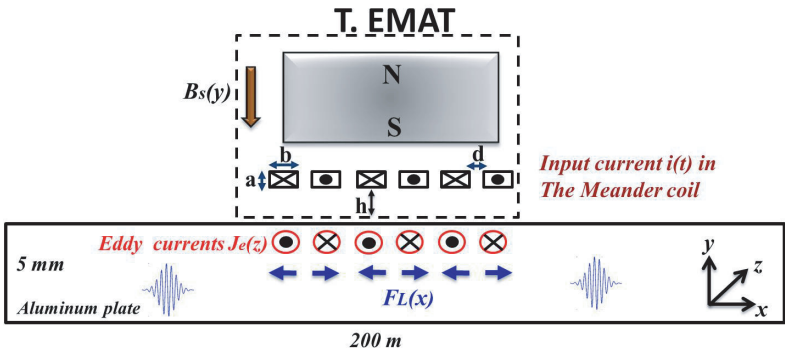


**Figure 1.** A schema represents configuration and the working principle of EMAT transmitter.

The geometrical and physical parameters of the EMAT configuration are given in Table 1. Figure 2 shows the input current density in the transmitter EMAT; $i_k(t)$ is expressed as:

$$i_k(t) = \beta e^{-\alpha(t-\tau)^2} \cos((4/3)\pi f(t-\tau)) \quad (1)$$

**Table 1.** Physical and geometrical parameters of EMAT.

| Symbol | Quantityl | value |
|---|---|---|
| $\sigma$ | Conductivity [S/M] | $3.7 \times 10^7$ |
| $B_r$ | Magnetic density [T] | 1.5 |
| $a$ | Coil thickness [mm] | 0.1 |
| $b$ | Coil width [mm] | 1 |
| $d$ | Coil distance [mm] | 2 |
| $h$ | Lift off distance [mm] | 1 |

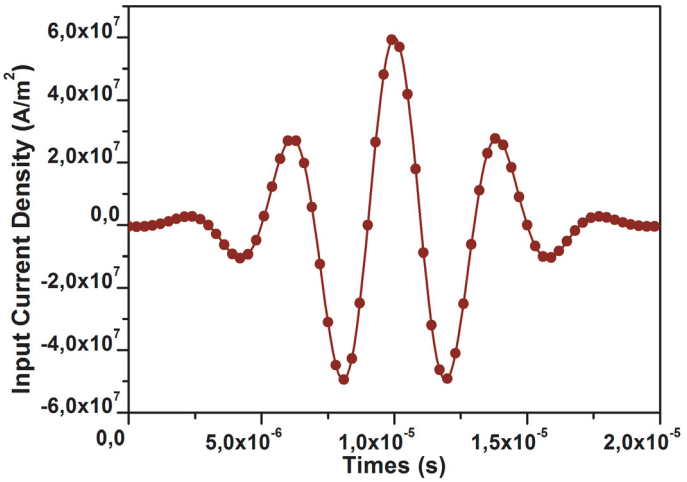


**Figure 2.** Input current density in the coil of the EMAT transmitter.

where $\beta$ is the amplitude (6 A), $\alpha$ the bandwidth factor ($5e^{-10}\,\mathrm{s}^{-2}$), $\tau$ the arrival time ($10^{-6}$ s), and $f$ the current frequency (400 kHz).

## 3. THE ELECTROMAGNETIC MODEL

### 3.1. The Governing Equations

The Maxwell equations are used to calculate the distribution of the induced eddy currents and the static magnetic field at the surface of the aluminum plate. The results are, then, used to evaluate the Lorentz force. The equation that governs the electrodynamic problem may be stated in terms of two unknowns: the electric scalar potential $V$ and the Magnetic Vector Potential (MVP) $\boldsymbol{A}_z$. The MVP $\boldsymbol{A}_z$ has only $z$-component, assuming that the material is infinitely long. The Maxwell's equations (Faraday's law and Ampere's law) that describe the electromagnetic model are defined as [15]:

$$\nabla \times \boldsymbol{H} = \boldsymbol{J} + \frac{\partial \boldsymbol{D}}{\partial t} \tag{2}$$

$$\nabla \times \boldsymbol{E} = -\frac{\partial \boldsymbol{B}}{\partial t} \tag{3}$$

where $\boldsymbol{E}$ is the electric field, $\boldsymbol{B}$ the magnetic flux density, $t$ the time variable, $\boldsymbol{H}$ the magnetic field strength, $\boldsymbol{J}$ the total current density, and $\boldsymbol{D}$ the electric flux density. If the EMAT frequency is not higher than several MHz, the term $\frac{\partial \boldsymbol{D}}{\partial t}$ in Maxwell's equations could be neglected.

According to Gauss' law and Faraday's law, the magnetic field and electric field can be defined in

terms of (MVP) $\boldsymbol{A_z}$ and the electric scalar potential $V$ as follows:

$$\boldsymbol{B} = \nabla \times \boldsymbol{A_z} \tag{4}$$

$$\boldsymbol{E} = -\nabla V - \frac{\partial \boldsymbol{A_z}}{\partial t} \tag{5}$$

The constitutive equations are defined as:

$$\boldsymbol{B} = \mu \boldsymbol{H} + \boldsymbol{B_r} \tag{6}$$

$$\boldsymbol{J} = \sigma \boldsymbol{E} + \sigma v \times (\nabla \times \boldsymbol{A_z}) \tag{7}$$

The magnetic field density formula in Eq. (4) and the electric field formula in Eq. (5) have been replaced in Equations (6) and (7), respectively, and become:

$$\boldsymbol{H} = \frac{1}{\mu}(\nabla \times \boldsymbol{A_z} - B_r) \tag{8}$$

$$\boldsymbol{J} = \sigma \left( -\nabla V - \frac{\partial \boldsymbol{A_z}}{\partial t} \right) + \sigma v \times (\nabla \times \boldsymbol{A_z}) \tag{9}$$

The formula of the magnetic field strength in Eq. (8) and the total current density in Eq. (9) have been substituted in the Ampere's law Equation (2). After some manipulations, we get the following Partial Deferential Equation (PDE) [16]

$$\nabla \times \left( \frac{1}{\mu} (\nabla \times \boldsymbol{A_z} - B_r) \right) + \sigma \frac{\partial \boldsymbol{A_z}}{\partial t} - \sigma v \times (\nabla \times \boldsymbol{A_z}) + \sigma \nabla V = \boldsymbol{J}_{ex} \tag{10}$$

where $\sigma$, $\mu$, $v$, and $\boldsymbol{J}_{ex}$ are conductivity, permeability, velocity, and external current density of the $k_{th}$ coil, respectively.

Equation (10) that governs the electromagnetic problem is numerically solved by the software COMSOL multiphysics based on the FEM method. COMSOL multiphysics is also used to model the mechanical problem. Eventually, this software allows the combination of the electromagnetic and the mechanical models. The electromagnetic part is solved by the 2D generic PDE mode using the static and transient analysis.

### 3.2. Lorentz Force Evaluation

The Lorentz force is considered as the driving source of the mechanical vibration within the material under test. The modeling of the electromagnetic model in the software COMSOL Multiphysics starts by the selection of the module which corresponds our physical problem. Before starting the electromagnetic modeling in static and transient analysis, the following elements should be defined; the boundary condition and the physical properties of the aluminum material, permanent magnet, and meanderline coil in the software COMSOL Multiphysics. Moreover, the time steps, relative tolerance, and absolute tolerance of the FEM model are also adjusted to obtain more precise results [17]. The static magnetic no-current of the AC/DC module is selected in order to calculate the static magnetic field at the surface of the aluminum plate. The solving of the PDE Equation (10) in the static analysis allows the calculation of (MVP) $\boldsymbol{A}_z$, which is used to evaluate the magnetic flux density $\boldsymbol{B_s}$ at the surface of the aluminum plate, as stated in Equation (4).

The transient analysis, which employs AC/DC quasi-static magnetic temporal module, is implemented to calculate the induced current $\boldsymbol{J_e}$ in the conductive material. The induced eddy current is principally limited in the skin depth of the aluminum plate. The MVP based on the PDE Equation (10) is solved in the transient model, and it is used to evaluate the induced current. The eddy current density $\boldsymbol{J_e}$ is defined according to the following equations:

$$\boldsymbol{J_e} = -\sigma \frac{\partial \boldsymbol{A_z}}{\partial t} \tag{11}$$

The Lorentz force $\boldsymbol{F_L}$ is produced through the interaction between the eddy current density $\boldsymbol{J_e}$ and the magnetic flux density $\boldsymbol{B_s}$, which are calculated in transient and static analysis. The Lorentz force is expressed according to the equation below [11].

$$\boldsymbol{F_L} = \boldsymbol{J_e} \times \boldsymbol{B_s} \tag{12}$$

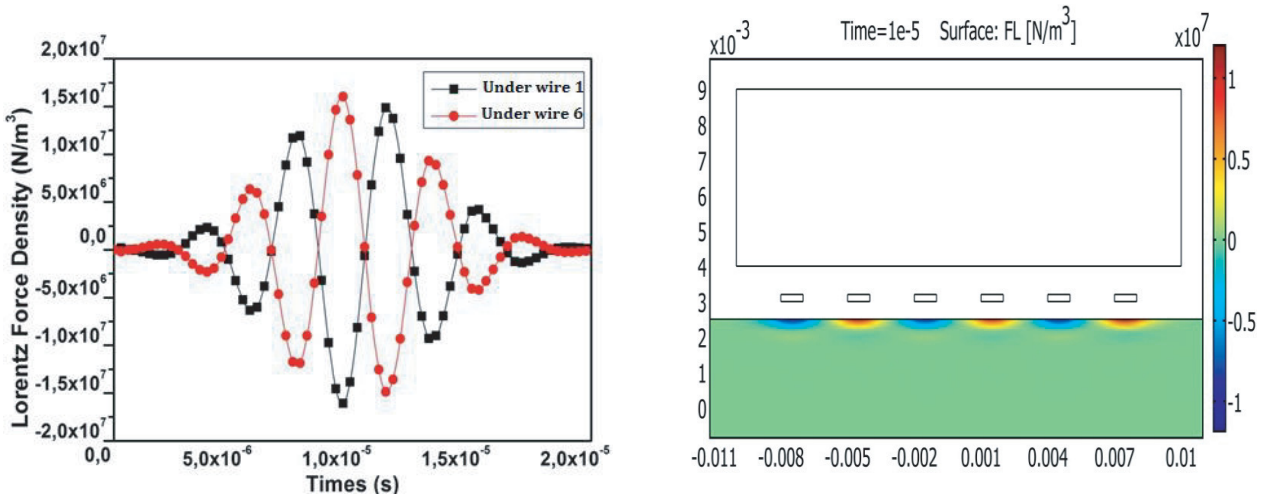


**Figure 3.** (a) The Lorentz force density. (b) The Lorentz force distribution at the surface of the aluminum plate.

The results shown in Figure 3 illustrate that the Lorentz force signal has the same waveform as the input current signal. Furthermore, the Lorentz force has the same density underneath wire 1 and 6, but in opposite directions. The Lorentz force that comes out of the dynamic magnetic field is ignored, because the dynamic magnetic field is always considered small compared to the external static magnetic field [14].

## 4. THE MECHANICAL MODEL

The electromagnetic and mechanical models are coupled by the Lorentz force, which applies an elastic deformation on the material under test. By considering that the material is linearly elastic, homogeneous, and isotropic, the motion equation is given as [17]:

$$\rho\frac{\partial^2 \boldsymbol{u}}{\partial t} = \nabla \cdot \boldsymbol{T} + \boldsymbol{F_L} \tag{13}$$

where $\boldsymbol{T}$ is the stress tensor, $\boldsymbol{u}$ the particle displacement vector, and $\rho$ the material density. According to the relationship between $\boldsymbol{T}$ and $\boldsymbol{u}$, Eq. (10) can be described as:

$$\mu\nabla \times \nabla \times \boldsymbol{u} - (\lambda + 2\mu)\nabla\nabla.\boldsymbol{u} + \rho\frac{\partial^2 \boldsymbol{u}}{\partial t} = \boldsymbol{F_L} \tag{14}$$

where $\lambda$ and $\mu$ are the Lame constants, and $\rho$ is the material density.

The mechanical model is built in the structural mechanics module of the software COMSOL multiphysic in order to solve the unknown particle displacement $\boldsymbol{u}$ in Equation (14). The ultrasonic wave is generated in an aluminum plate, with a length of 100 mm and a thickness of 5 mm. The plate under test has the following physical properties: a Youngs modulus of 70 GPa, a Poissons ratio of 0.33, and a mass density of 2700 kg/m$^3$.

In this section, the sensitivity of the EMAT system to the presence of the defects at the surface the aluminum plate has been checked. A defect is established at the surface of the aluminum plate, 25 mm away from the transmitter EMAT. The model is checked for three test run with three different sizes of the defect (see Figure 4(b)). The amplitude of the mechanical displacement $\boldsymbol{u}(t)$ signal on the material (under the receiver EMAT) is recorded for the different sizes of the defect proposed for the test. The results shown in Figure 4(a) represent the mechanical displacement on the aluminum plate in the $x$ direction. The results prove that the model is able to detect the changes in the defect size. That is effectively proportional to the reflection caused by the presence of the defect, which prevents the waves from being transmitted to the receiver.

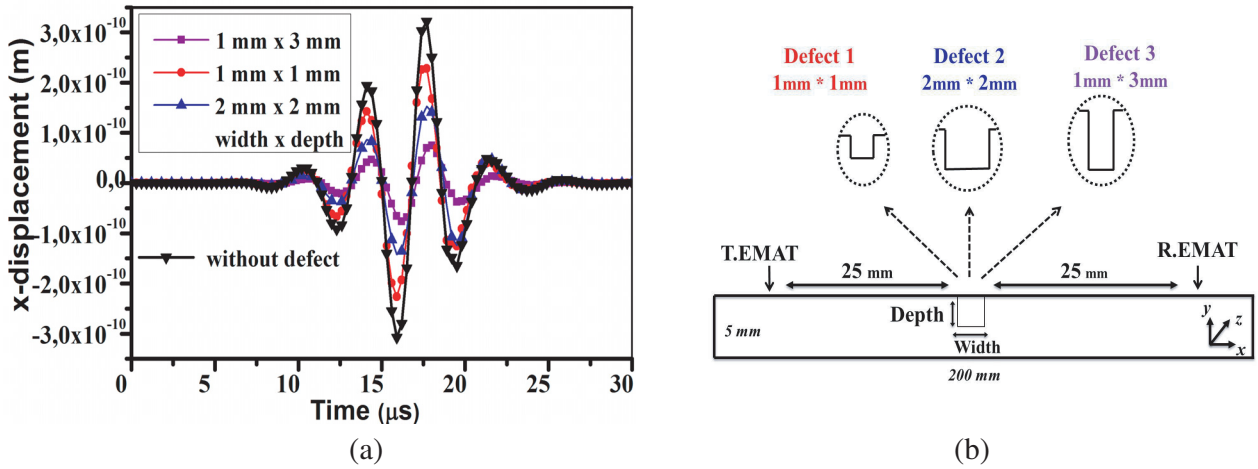


**Figure 4.** (a) The mechanical displacement at the surface of the aluminum plate for different defect sizes. (b) Cross section of 2D aluminum plate with surface defect.

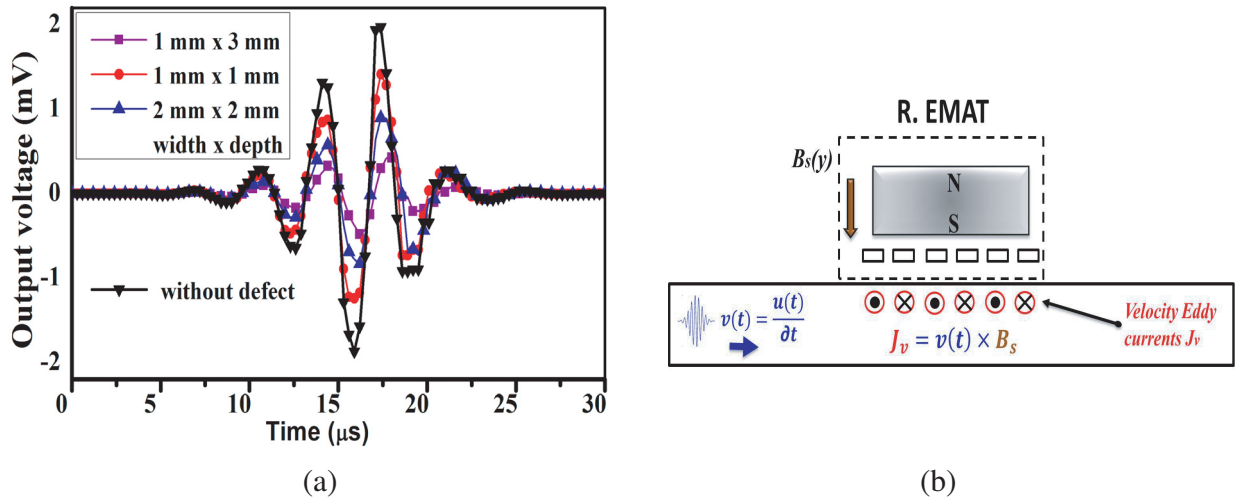


**Figure 5.** (a) The output voltage in the receiver EMAT for different defect sizes. (b) A schema represents the working principle and configuration of EMAT receiver.

In order to calculate the output voltage in the receiver EMAT, the electromagnetic model, which was previously developed, can be employed in reverse, where the excitation current $\boldsymbol{J_v}$ is outside of the receiver coil (see Figure 5(b)). The current sources are spatially distributed at the surface of the aluminum plate underneath the EMAT receiver, which results from the interaction of the velocity of the mechanical displacement $\boldsymbol{v}(t)$ that was calculated in the acoustic model, and the magnetic flux density $\boldsymbol{B_s}$ that comes from the EMAT receiver. These currents can induce a voltage in the coil of the EMAT receiver [8]. The results in Figure 5(a) represent the output voltage in the receiver and illustrate that the received signal has a similar waveform as the mechanical displacement. In addition, it is shown that the output signal can also be influenced by the change in the defect size at the surface of the aluminum plate.

## 5. THE INVERSE PROBLEM

In this section, an inverse problem is built in order to deduce the unknown geometrical parameters of the defect, based on the output voltage from the EMAT receiver (see Figure 6). The inverse problem can

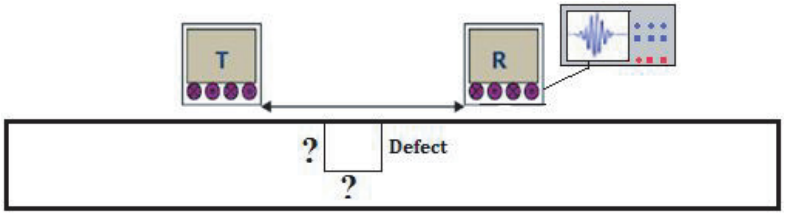


**Figure 6.** A schema represents the problematic of defect identification.

be solved using the iterative methods. However, they require an evaluation to the objective function, repeatedly, which leads to significant computational efforts. As a result, some methods based on artificial intelligence have been developed such as Adaptive Network based Fuzzy Inference System (ANFIS) and Artificial Neural Networks (ANN). However, ANFIS needs a relatively small database, and further, the number of membership functions and the parameters of the learning algorithm must be fixed. ANN is an efficient nonlinear statistical data modeling tool, but the over-fitting problem must be avoided. In addition, it needs an adjustment of the parameters of the back propagation learning algorithm [18, 19]. In this research, an efficient technique for dimensionality reduction called the Partial Least Square Regression (PLSR) method is proposed to find the relationship between defect dimensions and EMAT output voltage. PLSR is effective with multidimensional response problems with noisy data and correlated independent variables. Furthermore, it is convenient for the application to large data sets. Hence, these properties make the PLSR method more appropriate to solve the inverse problem.

### 5.1. PLSR Technique

PLSR technique functions as a dimensionality reduction method based on feature extraction and a multiple linear regression, through extracting a new set of uncorrelated components from the predictors $\boldsymbol{X}$, called latent variables (LV) [12, 13]. In the estimation of defect dimensions, PLS regression is used to find the fundamental relationship between two matrices, $\boldsymbol{X}$ and $\boldsymbol{Y}$. Let us consider a given predictors set $\boldsymbol{X}(x_1,\ x_2,\ dots,\ x_p)$ representing the EMAT output voltage, and the unknown defect dimensions are $\boldsymbol{Y}(y_1,\ y_2,\ dots,\ y_R)$, where $x_p$ is the $P^{th}$ independent variable, and $y_R$ is the $R^{th}$ dependent variable put in the same form as $x_p$. After observing $N$ samples from each set of the variables, PLS decomposes the predictors matrix $\boldsymbol{X}$ $(N \times P)$ and the output matrix of variables $\boldsymbol{Y}$ $(N \times R)$ into the following form

$$\boldsymbol{X} = \boldsymbol{T}\boldsymbol{P}' + \boldsymbol{E} \tag{15}$$

$$\boldsymbol{Y} = \boldsymbol{T}\boldsymbol{Q}' + \boldsymbol{F} \tag{16}$$

where the superscript denotes the transpose of the matrix; $\boldsymbol{T}$ is an $(N \times A)$ matrix of the $A$ extracted score vectors (components, latent vectors) for both predictors and responses, $\boldsymbol{P}(P \times A))$; $\boldsymbol{Q}(R \times A)$ represent the matrices of loadings. $\boldsymbol{E}(N \times P))$ and $\boldsymbol{F}(N \times R)$ are the matrices of residuals. The complete PLSR model gives $\boldsymbol{Y}$ in the function of $\boldsymbol{X}$ as follows (the residual matrix $\boldsymbol{F}$ is negligible):

$$\boldsymbol{Y} = \boldsymbol{X}\boldsymbol{B}_{\boldsymbol{PLS}} + \boldsymbol{F} \tag{17}$$

with $\boldsymbol{B}_{PLS}$ is the PLS regression coefficient matrix of $P + 1$ rows and $R$ columns.

### 5.2. Application and Results

The database required to fit the PLS model is created by solving the forward problem to get a set of output voltages from the receiver transducer, in which each pair of depth and width of the defect corresponds to its output signal. The database is generated by varying defect dimension (depth and width) in a random manner (300 examples); the defect depth ranges from 0.1 mm to 3 mm, and the defect width ranges 0.1 mm to 2 mm. For each assumed defect size, the received signal $\boldsymbol{V}(t)$ is recorded. The obtained data sets are divided into two subsets. The first subset (2/3) is used for the calibration of the PLS models and the selection of the appropriate number of LV, and the second subset (1/3) is used for testing and assessing the performances of the EMAT invers model.

In order to improve the accuracy and efficiency of the inversion model by PLSR method, it is necessary to obtain the optimal number of LV which is determined by implementing the cross-validation (CV) technique. the CV is applied to select the appropriate components which help to avoid over-fitting caused by the use of too large dimensional models. The choice of the LV optimal number is determined in the validation set, in which the increase of the number of LV does not show a significant difference of the Cross Validation-Root Mean Squared Error (CV-RMSE). The CV-RMSE obtained in the validation set in terms of the number of PLS components is illustrated in Figure 7. It is expressed as:

$$\mathrm{RMSE} = \sqrt{\frac{1}{N}\sum_{i=1}^{N}(y_i - \hat{y}_i)^2} \tag{18}$$

where $y_i$ is the value of the defect size, and $\hat{y}_i$ is the value of the PLSR prediction. According to the RMSE expression, it can be said that the unit of the RMSE is the same unit of the unknown defect dimensions (mm).

From the results shown in Figure 7, it can be noticed that the model has 38 significant components that have an effective influence on the predictive ability of the model. In addition to the CV-RMSE, another important measurement parameter of the model is the coefficient of determination $R^2$; it is evaluated for the calibration and the test sets.

$$R^2 = \frac{\left(\sum_{i=1}^{N}(y_i - \bar{y}_i)\left(\hat{y}_i - \bar{\hat{y}}_i\right)\right)^2}{\sum_{i=1}^{N}(y_i - \bar{y}_i)^2 \sum_{i=1}^{N}\left(\hat{y}_i - \bar{\hat{y}}_i\right)^2} \tag{19}$$

where $\bar{y}_i$ and $\bar{\hat{y}}_i$ are the mean of $y_i$ and $\hat{y}_i$, respectively, and $N$ is the number of examples in the data set.

Figure 8(a) shows the ratio $\mathrm{Var}(\boldsymbol{T}P')/\mathrm{Var}(\boldsymbol{X})$ that represents the variance of $\boldsymbol{X}$ dividing one of its PLS approximations ($\boldsymbol{T}P'$), in function of the number of PLS components retained. This graph shows that the first 10 components contain more than 98% of the original predictors variance. Figure 8(b) shows the same thing as the approximation of the response $\boldsymbol{Y}$: $(\boldsymbol{T}Q')/\mathrm{Var}(\boldsymbol{Y})$. In order to test the efficiency of the proposed inversion model in terms of predictive accuracy, the PLSR technique is applied to the test set with the optimal number of LV (38).

Figures 9 and 10 show a comparison between the defects provided by PLSR technique and those in the calibration and test sets. It can be seen that the points in each figure are clustered around a straight line with the same slope, which means that the estimated defects sizes are almost equal to the desired

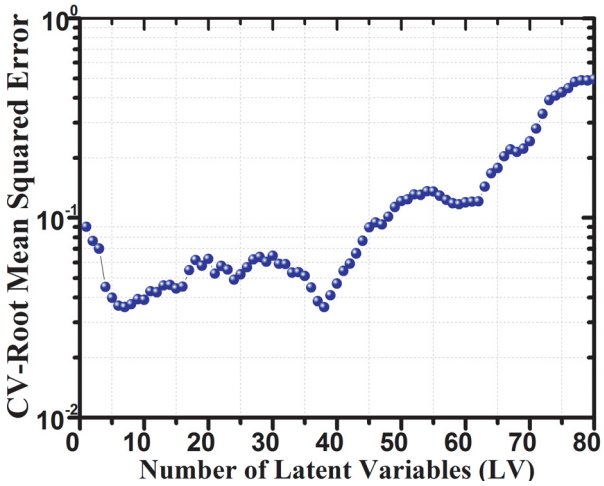


**Figure 7.** The average of RMSE on the validation sets.

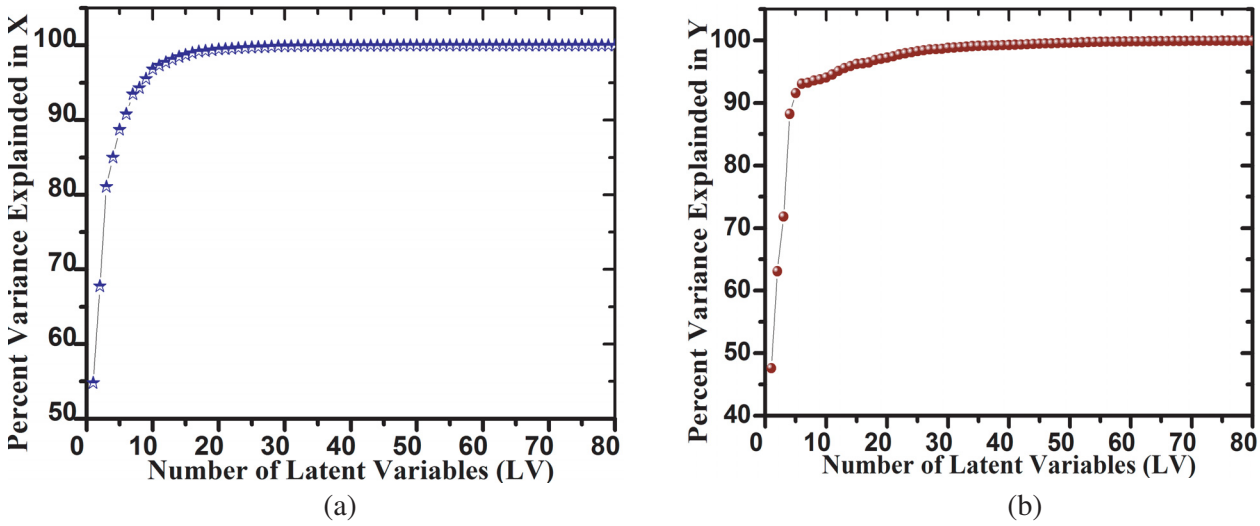


**Figure 8.** Percentage of the variance; (a) for X set, (b) for Y set are explained by the PLS analysis.

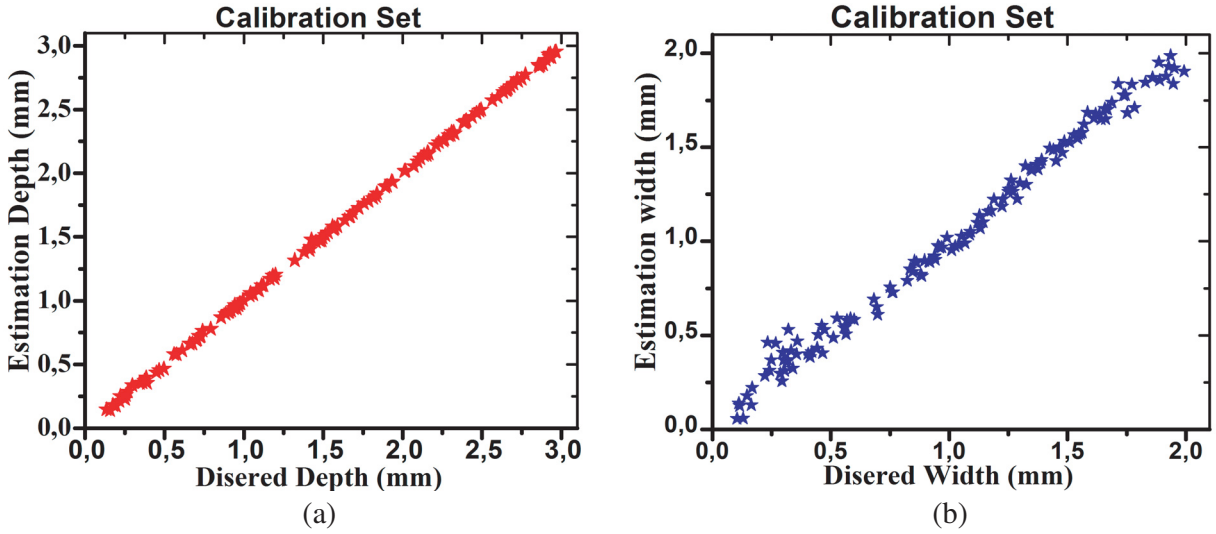


**Figure 9.** Comparison between desired and estimated values in the calibration set: (a) for the defect depth (b) for the defect width.

ones. Moreover, the obtained results in Table 2 show a very low value of the RMSE of prediction, which demonstrates a very good predictive accuracy. Furthermore, the values of $R^2$ are higher than 0.9, which indicates that the model can gain a better prediction performance.

**Table 2.** The expected and the obtained geometrical defect parameters.

| Calibration Set | | Test Set | | Depth (mm) × Width (mm) | |
|---|---|---|---|---|---|
| RMSE | R2 | RMSE | R2 | Expected | Obtained |
| $5.01\times10^{-5}$ | 0.997 | $7.01 \times 10^{-5}$ | 0.994 | $1.21 \times 1.2$<br>$2.74 \times 0.27$ | $1.20 \times 1.30$<br>$2.78 \times 0.24$ |

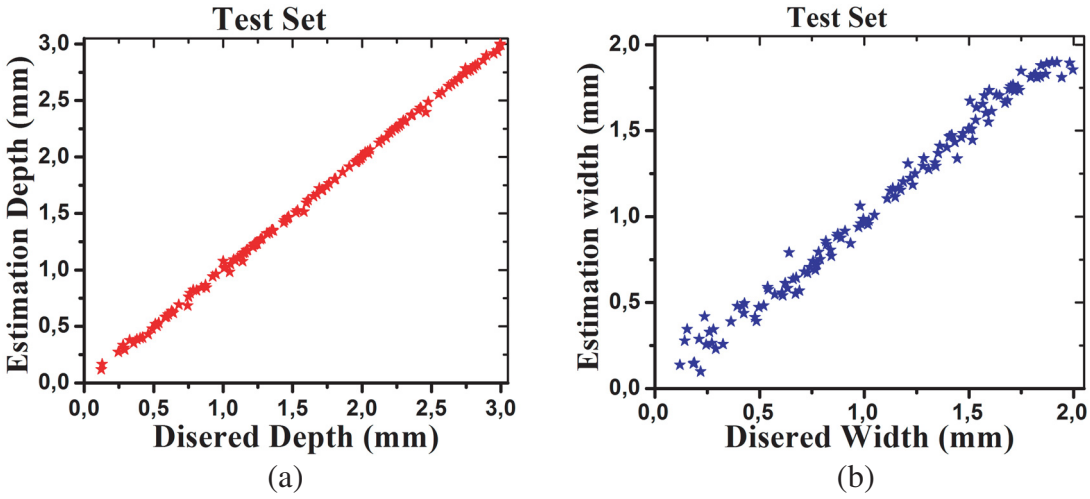


**Figure 10.** Comparison between desired and estimated values in the test set: (a) for the defect depth, (b) for the defect width.

## 6. CONCLUSION

In this work, PLSR technique and EMAT technology are combined in order to estimate the defect dimensions (depth and width) at the surface of an aluminum plate. The FEM method is applied to build a forward problem, which includes a combination of the electromagnetic and mechanical models. In the electromagnetic model, the Lorentz force is produced through the interaction of the magnetic field and the induced eddy current at the surface of the aluminum plate. the Lorentz force serves as the source of the elastodynamic model, which involves a propagation of the mechanical displacement within the material. According to the obtained results, the forward model illustrates that the EMAT system has a high sensitivity to the existence or the change in the size of the defects. The EMAT system has proved that the arriving mechanical displacement can be detected by the EMAT receiver as an output voltage in its coils. Finally, the PLSR method is used to solve EMAT inverse problem, which is represented as an estimation of the unknown defect size by employing the database of the output voltage. The achieved results prove the efficiency of the adopted approach to deduce defect size and encourage further work on this subject.

## REFERENCES

1. Burrascano, P., S. Callegari, A. Montisci, M. Ricci, and M. Versaci, "Ultrasonic nondestructive evaluation systems: Industrial application issues," *Springer*, 1–4, 2015.
2. Dhayalan, R. and K. Balasubramaniam, "A two-stage finite element model of a meander coil electromagnetic acoustic transducer transmitter," *Nondestructive Testing and Evaluation*, Vol. 26, No. 02, 101–118, 2011.
3. Yi, P., K. Zhang, Y. Li, and X. Zhang, "Influence of the lift-off effect on the cut-off frequency of the EMAT-generated rayleigh wave signal," *Sensors*, Vol. 14, No. 10, 19687–19699, 2014.
4. Edwards, R., S. Dixon and X. Jian, "Enhancement of the Rayleigh wave signal at surface defects," *Journal of Physics D: Applied Physics*, Vol. 37, No. 16, 2291–2297, 2004.
5. Mirkhani, K., et al., "Optimal design of EMAT transmitters," *NDT & E International*, Vol. 37, No. 3, 181–193, 2004.
6. Jafari-Shapoorabadi, R., A. Konrad, and A. Sinclair, "Improved finite element method for EMAT analysis and design," *IEEE Transactions on Magnetics*, Vol. 37, No. 4, 2821–2823, 2001.
7. Thompson, R., "A model for the electromagnetic generation and detection of rayleigh and lamb waves," *IEEE Transactions on Sonics and Ultrasonics*, Vol. 20, No. 4, 340–346, 1973.

8. Ludwig, R., Z. You, and R. Palanisamy, "Numerical simulations of an electromagnetic acoustic transducer-receiver system for NDT applications," *IEEE Transactions on Magnetics*, Vol. 29, No. 3, 2081–2089, 1993.
9. Murray, P. and R. Dewhurst, "Application of a laser/EMAT system for using shear and LS mode converted waves," *Ultrasonics*, Vol. 40, Nos. 1–8, 771–776, 2002.
10. Jian, X., S. Dixon, K. Grattan, and R. Edwards, "A model for pulsed Rayleigh wave and optimal EMAT design," *Sensors and Actuators A: Physical*, Vol. 128, No. 2, 296–304, 2006.
11. Dhayalan, R., V. Satya Narayana Murthy, C. Krishnamurthy, and K. Balasubramaniam, "Improving the signal amplitude of meandering coil EMATs by using ribbon soft magnetic flux concentrators (MFC)," *Ultrasonics*, Vol. 51, No. 6, 675–682, 2011.
12. Wold, H., "Partial least squares," *Encyclopedia of Statistical Sciences*, S. Kotz and N. L. Johnson, Eds., Vol. 6, 581–591, John Wiley, New York, 1985.
13. Sadou, H., T. Hacib, Y. Le Bihan, O. Meyer, and H. Acikgoz, "Predictors generation by partial least square regression for microwave characterization of dielectric materials," *Physica B: Condensed Matter*, Vol. 550, 2018.
14. Ribichini, R., F. Cegla, P. Nagy, and P. Cawley, "Study and comparison of different EMAT configurations for SH wave inspection," *IEEE Transactions on Ultrasonics, Ferroelectrics and Frequency Control*, Vol. 58, No. 12, 2571–2581, 2011.
15. Itaya, T., K. Ishida, Y. Kubota, A. Tanaka, and N. Takehira, "Visualization of eddy current distributions for arbitrarily shaped coils parallel to a moving conductor slab," *Progress In Electromagnetics Research M*, Vol. 47, 1–12, 2016.
16. Kaltenbacher, M., R. Lerch, H. Landes, K. Ettinger, and B. Tittmann, "Computer optimization of electromagnetic acoustic transducers," *Proc. IEEE Ultrason. Symp.*, Vol. 2, 1029–1034, Oct. 1998.
17. Wang, S., S. Huang, Y. Zhang, and W. Zhao, "Multiphysics modeling of a lorentz force-based meander coil electromagnetic acoustic transducer via steady-state and transient analyses," *IEEE Sensors Journal*, Vol. 16, No. 17, 6641–6651, 2016.
18. Morabito, E. and M. Versaci, "A fuzzy neural approach to localizing holes in conducting plates," *IEEE Transactions on Magnetics*, Vol. 37, No. 5, 3534–3537, 2001.
19. Chelabi, M., T. Hacib, Y. Le Bihan, N. Ikhlef, H. Boughedda, and M. Mekideche, "Eddy current characterization of small cracks using least square support vector machine," *Journal of Physics D: Applied Physics*, Vol. 49, No. 15, 155303, 2016.